Subsonic Aerodynamic Performance of Nozzle Installations in Supersonic Airplanes

R. S. ARMSTRONG* AND S. R. MILLER†
The Boeing Company, Renton, Wash.

The external aerodynamic performance of supersonic airplane nozzle systems at subsonic speeds is studied and some significant results of analytical and experimental investigations of exhaust system subsonic drag are shown. Experimental techniques are described which can minimize model scaling uncertainties in wind-tunnel tests. An analysis method for successfully predicting drag on axisymmetric bodies at subsonic speeds combines axisymmetric potential flowfield predictions with laminar and turbulent boundary-layer computation procedures. The results for certain applications are compared with experiment, and application of the analysis to the design of asymmetric models for detailed experimental investigations is demonstrated. For accurate extension of model test results to full-scale airplane performance predictions, an analytical method is proposed. This discussion concludes with a mention of some limitations of the analysis and of areas where further work is needed.

Nomenclature

A_π = model cross-sectional area
C_D = drag coefficient = D/qA_π
C_P = pressure coefficient = $(P_L - P)/q$
D = drag
F_{ideal} = ideal isentropic nozzle thrust
L = model length
M = Mach number
P = freestream static pressure
P_L = local static pressure
P_T = nozzle total pressure
$P_{T_{BL}}$ = boundary-layer local total pressure
q = dynamic pressure = $\gamma PM^2/2$
u = local velocity
U_∞ = freestream velocity
X = pressure tap location
Y = coordinate normal to the model surface
γ = ratio of specific heats
δ^* = boundary-layer displacement thickness = $\int_{Y=0}^{\infty}\left(1 - \frac{u}{U_\infty}\right) dY$
θ = boundary-layer momentum thickness = $\int_{Y=0}^{\infty} \frac{u}{U_\infty}\left(1 - \frac{u}{U_\infty}\right) dY$

Introduction

MANY new airplanes designed to fly at supersonic speeds are required to fly long distances at high subsonic speeds during a mission. The engines of these aircraft normally require afterburning power settings to provide sufficient thrust for supersonic operation; however, nonafterburning power settings are usually employed for subsonic operation. Figure 1 shows a tactical fighter with an afterburning engine in two flight regimes. As shown in the figure, the nozzle exit area is large during supersonic flight and small during subsonic flight. This means that a large boattail or base area exists on the airplane during subsonic flight. If the nozzle system installation is faulty, the large boattail area can cause a significant drag increase and consequent reduction of mission range.

Presented as Paper 67–452 at the AIAA 3rd Propulsion Joint Specialist Conference, Washington, D.C., July 17–21, 1967; submitted August 22, 1967; revision received February 21, 1968.

* Research Specialist, Commercial Airplane Division.
† Research Engineer, Commercial Airplane Division.

Published investigations of aerodynamic performance of nozzle systems at subsonic speeds have emphasized the experimental approach to design of nozzle installations. There are, however, two major problems in the application of wind-tunnel test results to full-scale airplanes—the uncertainty of scaling effects and the uncertainty of accuracy of absolute drag levels as measured in wind tunnels. Drag analysis methods that can provide information on scaling effects are available, but they are limited to axisymmetric bodies and are not capable of adequately handling the problems of separated flow and jet entrainment.

This report presents a combined analytical and experimental approach to the investigation of the external aerodynamic performance of supersonic airplane-nozzle systems at subsonic speeds. The diagram of Fig. 2 outlines the procedure. A test technique that leads to accurate drag data relative to a reference body which is amenable to analysis is described. An experimental method of measuring drag levels and an analytical verification are presented. An analytical method of scaling model test results to full scale, based on a reference model, is shown.

Nozzle System Drag and Mission Range

Two typical missions for the tactical fighter can be used to illustrate the effect of drag increase on mission range (Fig. 3). The aircraft must be able to fly at the supersonic speeds required for the intercept mission. However, a major requirement is the tactical support mission flown at subsonic speeds under nonafterburning conditions. For this reason, the

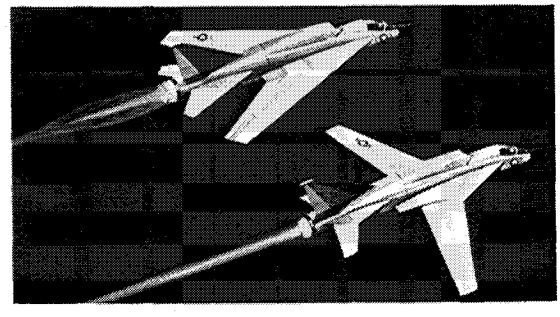

Fig. 1 Supersonic/subsonic flight.

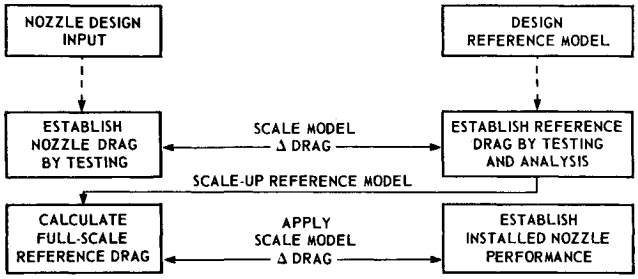

Fig. 2 Prediction of nozzle installation drag.

nozzle afterbody must be designed for the minimum possible subsonic drag while still satisfying supersonic flight requirements.

The significance of subsonic drag penalties for the tactical fighter mission is illustrated in Table 1, which shows how range loss and fuel consumption are related to each mission phase. Most of the mission fuel is consumed at the high subsonic Mach numbers, where the problem of the aerodynamic performance of the nozzle is most severe.

Scale-Model Testing

Wind-tunnel performance tests of isolated exhaust nozzles are of limited value in designing an integrated propulsion system for buried installations such as that of the single-engine fighter of Fig. 1. Wind-tunnel tests designed for the particular installation are required to account for airplane-nozzle system drag interactions. Proper simulation of nozzle systems in the wind tunnel requires consideration of the model scale, the degree of jet simulation required, and how much of the airplane must be included in the model.

Wind-tunnel blockage usually imposes restrictions on the test model size. As a result, the data are subject to uncertainties due to scaling effects, such as lack of simulation of Reynolds number and model boundary layer. Because most wind tunnels operate at or near sea-level pressures and temperatures, it is the usual practice to test at the proper Mach number but at lower than the desired Reynolds number. This causes the model to have larger regions of laminar boundary layer than do full-scale installations and, therefore, different drag.

Simulation of the nozzle exhaust plume is considered essential in installed nozzle tests because of jet interactions with the airplane surface and the effects of jet entrainment on the local flowfield. The jet plume shape varies with pressure ratio and Mach number. At supercritical pressure ratios, with convergent nozzles, the external flow is forced to turn away from the boattail to follow the jet plume shape. This turn causes the external flow near the body to decelerate and the static pressure in this region to increase. Figure 4 shows the local static pressure increase on a gentle boattail at Mach 0.8. As the nozzle pressure ratio is increased, the boattail pressures become more and more positive, and some pressure thrust is recovered because of the jet plume. In this case, if the jet

Table 1 Drag penalties for tactical fighter mission

Mission phase	Fuel used, %	Range loss for 10% drag increase, naut miles
Takeoff	8.0	...
Subsonic cruise	5.7	6
Subsonic approach	36.6	35
Subsonic escape	35.0	35
Subsonic cruise	5.0	6
Loiter	4.0	...
Landing	5.7	...

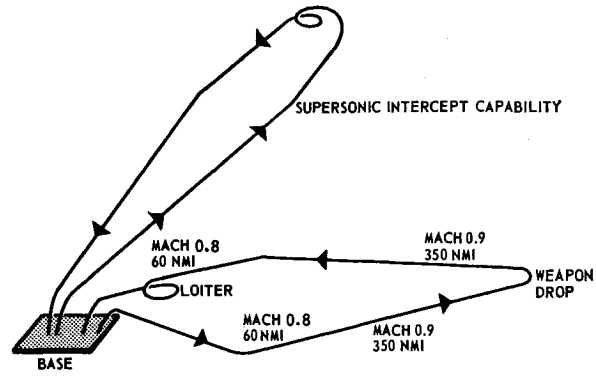

Fig. 3 Typical tactical fighter missions.

plume is not simulated, the nozzle boattail drag will be unrealistically high.

In addition, the effect of jet entrainment can affect the flowfield. Flow visualization tests on a steep boattail at Mach 0.92 with and without a propulsive jet produced the results shown in Figs. 5 and 6, respectively. The separated flow region is markedly reduced because of air entrainment by the jet. This potentially large effect of viscous mixing on afterbody performance is another strong argument for jet simulation in scale-model testing.

A Systematic Approach to Wind-Tunnel Testing

To minimize uncertainties due to scaling and incomplete airplane simulation, it is useful to determine effects of nozzle installation on a relative rather than an absolute basis. An idealized reference model is carefully designed so that its drag may be calculated theoretically. It is smoothly contoured to avoid possible separated flow regions and utilizes an efficient convergent nozzle uncompromised by the off-design requirements of practical nozzles. Therefore, the absolute drag level of the reference model can be more accurately established than the drag of practical models. The reference model drag is established by subtracting installed thrust-minus-drag measured in wind-tunnel tests from the measured static thrust of the nozzle. The reference model is then replaced by practical installation models whose drag is determined in the same manner. Finally, drag penalties for practical nozzle installations are determined as the difference between reference and practical configuration drags. When several wind-tunnel test series are to be run at different times, the same reference model is used each time. This will demonstrate repeatability in thrust-minus-drag levels and allow direct comparison of different nozzle installations even though the tests may be run at different times and at different locations.

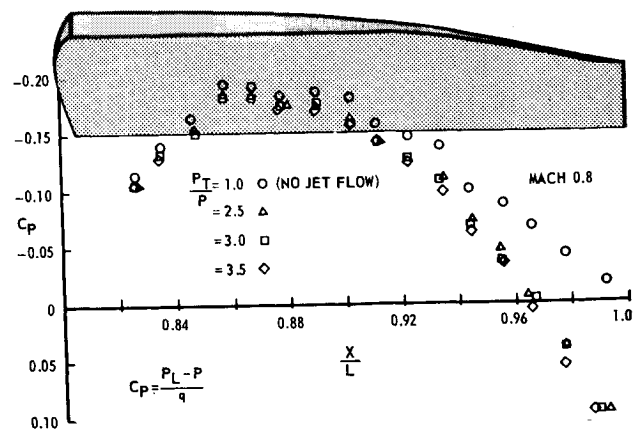

Fig. 4 Effect of jet on boattail pressure distribution.

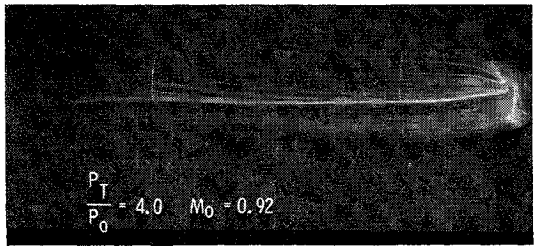

Fig. 5 Boattail separation with jet at a pressure ratio of 4.

Analysis Method

The reference test method described is useful for reducing uncertainties of model drag differences in wind-tunnel tests. Analysis techniques are required, however, to apply the absolute drag levels of the reference model to the prediction of full-scale nozzle installation drag. Test results may then be more confidently applied to airplane design.

The analysis method to be described makes possible the prediction of drag on axisymmetric bodies. The method combines potential flow and boundary-layer computations in the manner suggested by Granville.[1]

Axisymmetric potential flow theory corrected for compressibility effects can be used to predict the external pressure

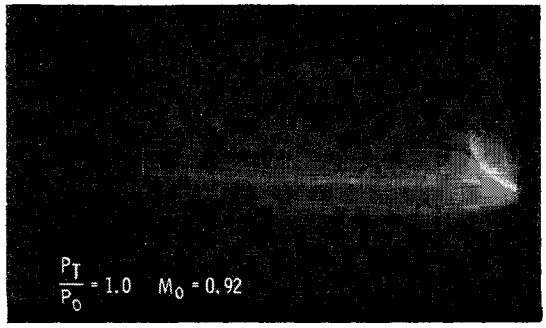

Fig. 6 Boattail separation with no propulsive jet.

distribution on axisymmetric bodies. Since the net force on a body in a wholly potential flow is zero, potential flow theory cannot be used to predict pressure drag. Boundary-layer growth must be considered in the analysis. Boundary-layer computation must consider laminar boundary-layer growth, transition, and turbulent boundary-layer growth. These are predictable from body shape and static pressure distribution.

Boundary-layer displacement thickness δ^* is a measure of the amount a surface must be displaced so that the effect of the boundary layer is reflected in the potential flowfield. A body in a flowfield can be mathematically represented if its

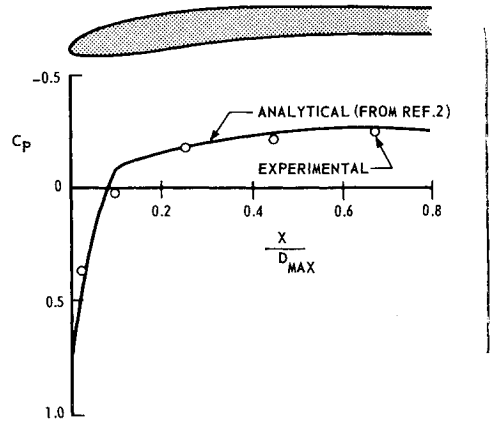

Fig. 7 Pressure distribution on cowl (Mach 0.4).

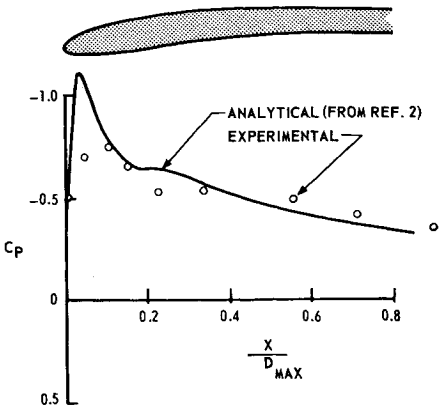

Fig. 8 Pressure distribution on cowl (Mach 0.7).

coordinates are displaced by δ^*, and the potential flow pressure distribution on this mathematical model can be computed. Application of the computed pressure distribution to the original body then yields the pressure drag of the model. In actual practice, this is an iterative process: the potential flow pressure distribution on the physical body is computed and used to obtain a boundary layer; displacement thickness is then added to the physical body, and a new pressure distribution and a new boundary layer are computed; the new displacement thickness is then added to the physical body. The

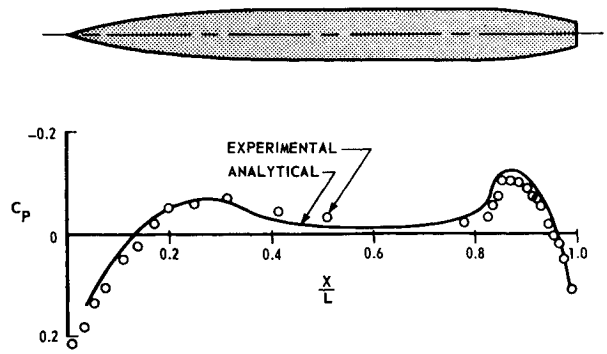

Fig. 9 Pressure distribution on axisymmetric body (Mach 0.5).

process is repeated until two iterations produce the same pressure distribution. The final boundary layer and static pressure distribution are used to determine skin friction and pressure drag on the model.

Comparison of Theory with Test Results

The potential flow analysis procedure used by the authors was an axisymmetric relaxation solution with a compressi-

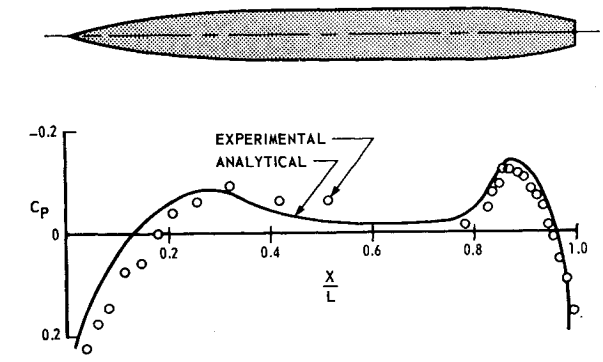

Fig. 10 Pressure distribution on axisymmetric body (Mach 0.8).

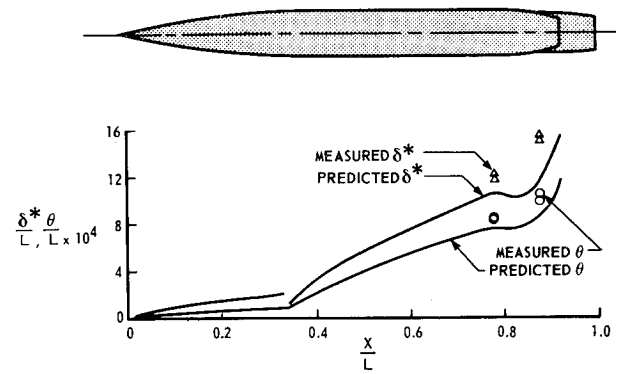

Fig. 11 Boundary-layer growth on axisymmetric body (Mach 0.5).

bility correction. The computation method used was developed by Colehour.[2] Analytical pressure distributions from Ref. 2 are compared with experimental data for two inlet cowls in Figs. 7 and 8. Pressure distributions on axisymmetric bodies are shown in Figs. 9 and 10. The method appears to predict reasonably good pressure distributions in both cases.

The boundary-layer analyses described in this paper were obtained from a Boeing computation method for prediction of

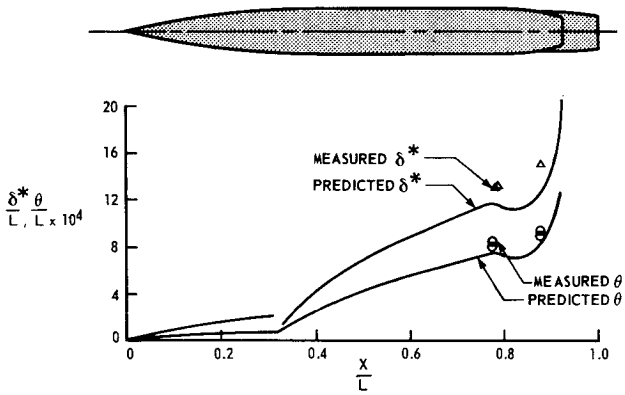

Fig. 12 Boundary-layer growth on axisymmetric body (Mach 0.8).

axisymmetric boundary-layer growth. The method of solution combines the laminar boundary-layer analysis of Launder[3] with the turbulent method of Granville.[4] Since the Launder solution is two-dimensional, the transformation from two-dimensional flow to axisymmetric flow proposed by Mangler[5] was incorporated in the analysis.

Analytical predictions of boundary-layer growth are compared with measurements made in the Boeing transonic wind in Figs. 11 and 12. Agreement is seen to be good. The experimental results were obtained by surveying the boundary

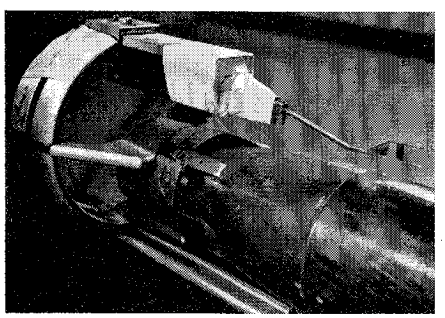

Fig. 13 Boundary-layer survey mechanism.

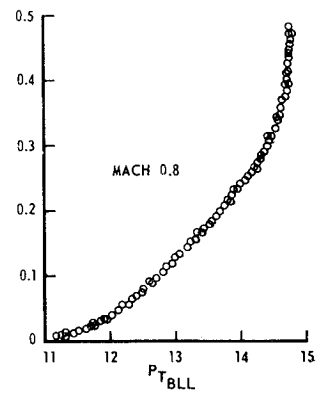

Fig. 14 Boundary-layer total pressure profile.

layer with the traversing mechanism shown in Fig. 13. A typical total pressure profile from the model is shown in Fig. 14. The velocity profile computed from the total pressure distribution is shown in Fig. 15. Displacement and momentum thicknesses were then obtained by performing the respective integrations over the boundary layer.

The drag iteration process was applied to a gently curved axisymmetric boattail model for which a cylindrical jet plume was assumed. Figure 16 shows the results of the analysis. Solid lines show conditions on the physical model, dashed lines show conditions on the body with displaced boundaries, and points show the measured model data. Consideration of displacement thickness is seen to shift the pressure coefficient curve closer to the measured data. The

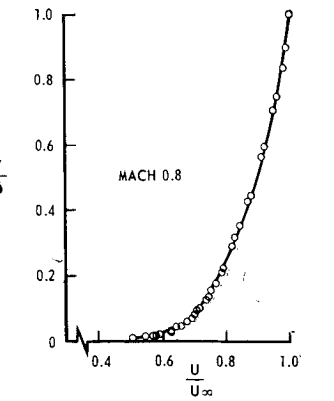

Fig. 15 Boundary-layer velocity profile.

iteration procedure changes conditions forward of the boattail a negligible amount.

When the final pressure distribution shown is used to determine boattail pressure drag, a value of pressure-drag coefficient of 0.017 is obtained. The boattail pressure drag coefficient obtained from test results was 0.018. The skin-friction drag coefficient of the forebody and boattail was

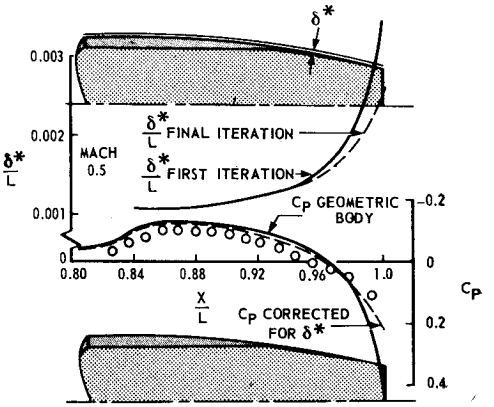

Fig. 16 Matching of viscous and potential flows near a body.

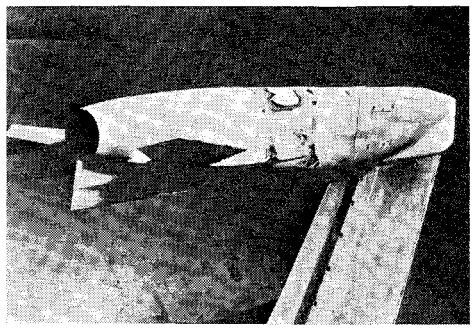

Fig. 17 Test model in transonic tunnel.

determined by analysis to be 0.098. Test results indicated the skin-friction drag coefficient to be 0.101.

These methods make possible the computer simulation and rapid study of a series of nozzle afterbodies on axisymmetric bodies. For cases such as a fighter, where the engine is buried in a definitely asymmetric fuselage, it will be shown that some nozzle trade studies may also be accomplished in the same manner. However, much more testing is required to confirm the analytical results because effects that are not predictable by axisymmetric analysis may be present.

Application of Analysis to Experimental Techniques

The test and analysis procedures that have been discussed were applied in a recent Boeing drag study. In wind-tunnel studies of the propulsion system installation for the fighter of Fig. 1, the reference model test technique described earlier was used. The reference model had to meet several requirements. The model was to be mounted on an air-supply strut, so it was necessary to integrate the model nacelle with the strut. It was also desirable to match as many of the airplane fuselage contours as possible. However, it was necessary to shorten the model forebody in order to obtain the desired boundary-layer characteristics at the start of the afterbody. The model is shown in Fig. 17.

After the reference model performance was established, the convergent nozzle was replaced by a series of possible nozzle installations having equal effective throat areas. The nozzles represented designs for an afterburning engine having a ratio of afterburning to nonafterburning nozzle throat area of 1.9. The performance of these practical configurations relative to the reference convergent nozzle was then determined. The results given in Fig. 18 show the relative performance of several of the nozzles designed for the example installation. They do not necessarily indicate the relative performance of these nozzles on another type of installation. The range

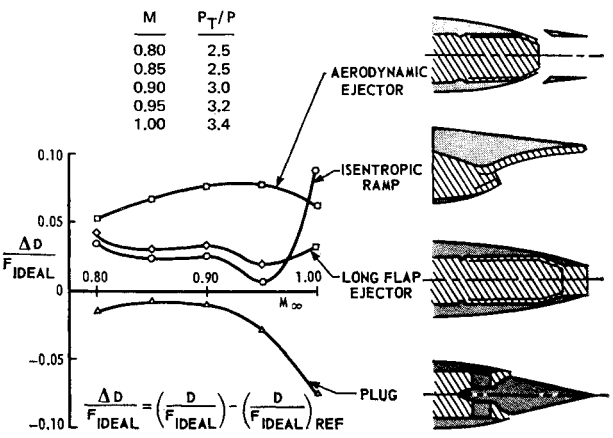

Fig. 18 Drag penalties for typical nozzles.

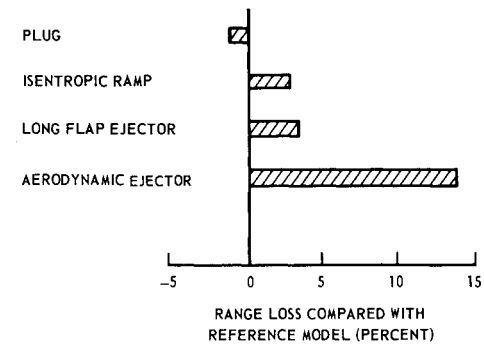

Fig. 19 Range penalties from nozzle system drag.

penalty that the drag of each of these nozzles would cause on the subsonic tactical fighter mission of Fig. 3 is given in Fig. 19. This figure does not reflect the total relative merits of these nozzles (as affected by additional factors such as weight, complexity, maintainability, length, etc.), but only points out the significance of drag differences and, therefore, the importance of nozzle system drag in evaluating the over-all relative merits of the nozzles.

At the conclusion of the test phase, the drag of the reference model (Fig. 17) was predicted. Since the analysis procedure requires an axisymmetric body, a mathematical representation of the real model with the same area distribution but with axisymmetric contours was made. (Although the flowfield may be different locally on the model, the total flow blockage at any point is correct; therefore, the over-all potential flowfield should be a reasonable representation of the flowfield around the asymmetric model.) The pressure and skin-friction drag on this representation were then predicted by the iteration procedure discussed earlier. The results of the iterations are shown in Fig. 20. A total drag coefficient of 0.092 (based on an $A\pi$ of 29.27 in.^{2}) was computed at Mach 0.8. This compares with the measured value of 0.089.

Prediction of Full-Scale Nozzle Installation Drag

These results suggest that an integrated test and analysis approach should make it possible to accurately predict nozzle installation drag. The initial step in the theoretical analysis is the simulation of the full-scale airplane with an axisymmetric body of equivalent area distribution. Pressure distribution and boundary-layer growth on this body are predicted by analysis. A wind-tunnel reference model is designed with a simple nozzle and an afterbody that matches the full-scale afterbody area distribution. The forebody length is then adjusted so that the ratio of boundary-layer displace-

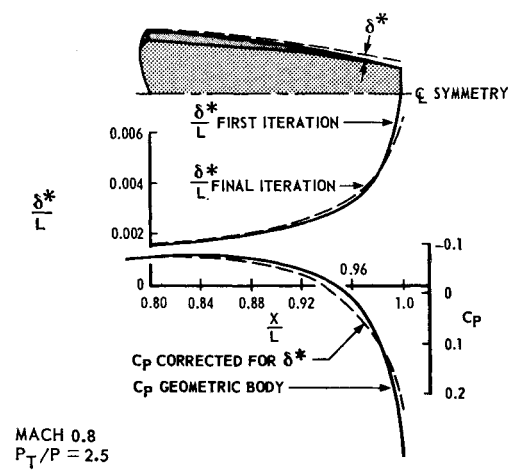

Fig. 20 Matching of viscous and potential flows of reference model.

ment thickness to model diameter at the beginning of the afterbody is similar to the predicted full-scale value, even though the wind-tunnel Reynolds numbers are different from the full-scale values. The drag of the wind-tunnel reference model is established by testing and confirmed by analysis. Practical configurations are wind-tunnel tested and compared with the reference model values. Full-scale nozzle installation drag is determined by computing the drag of the nozzle on the axisymmetric representation of the full-scale airplane through the analysis procedure described. The drag of a practical configuration is then predicted by adding the measured drag increment from model tests to the computed full-scale reference nozzle drag.

This procedure may help to reduce the uncertainties of present drag-prediction methods. However, several problem areas still exist. Available calculation procedures will not account for separated flow regions or jet entrainment effects at subsonic speeds. The application of axisymmetric body drag prediction methods is limited. An asymmetric solution is required to extend the analysis methods to more general airplane shapes.

References

[1] Granville, P. S., "The Calculation of the Viscous Drag of Bodies of Revolution," Rept. 849, July 1953, David Taylor Model Basin.

[2] Colehour, J. L., "A Relaxation Solution for Two-Dimensional and Axisymmetric Potential Flow Problems," D6-18087TN, June 21, 1966, The Boeing Co.

[3] Launder, B. E., "An Improved Pohlhausen-Type Method of Calculating the Two-Dimensional Boundary Layer in a Pressure Gradient," Paper 63-HT-26, Aug. 1963, American Society of Mechanical Engineers.

[4] Granville, P. S., "A Method for the Calculation of the Turbulent Boundary Layer in a Pressure Gradient," Rept. 752, May 1951, David Taylor Model Basin.

[5] Schlicting, H., *Boundary Layer Theory*, Pergamon, New York, 1955, p. 168.